REPORT DOCUMENTATION PAGE

Form Approved
OMB No. 0704-0188

1. REPORT DATE *(DD-MM-YYYY)*	**2. REPORT TYPE**	**3. DATES COVERED** *(From - To)*
20-06-2005	Technical Paper	

4. TITLE AND SUBTITLE

Experiments on a Coaxial Injector Under an Externally-Forced Transverse Acoustic Field (PREPRINT)

5a. CONTRACT NUMBER

5b. GRANT NUMBER

5c. PROGRAM ELEMENT NUMBER

6. AUTHOR(S)
D.W. Davis and B. Chehroudi (ERC, Inc.); D.G. Talley (AFRL/PRSA)

5d. PROJECT NUMBER
2308

5e. TASK NUMBER
0533

5f. WORK UNIT NUMBER

7. PERFORMING ORGANIZATION NAME(S) AND ADDRESS(ES)

Air Force Research Laboratory (AFMC)
AFRL/PRSA
10 E. Saturn Blvd.
Edwards AFB CA 93524-7680

8. PERFORMING ORGANIZATION REPORT NUMBER

AFRL-PR-ED-TP-2005-410

9. SPONSORING / MONITORING AGENCY NAME(S) AND ADDRESS(ES)

Air Force Research Laboratory (AFMC)
AFRL/PRS
5 Pollux Drive
Edwards AFB CA 93524-70448

10. SPONSOR/MONITOR'S ACRONYM(S)

11. SPONSOR/MONITOR'S NUMBER(S)
AFRL-PR-ED-TP-2005-410

12. DISTRIBUTION / AVAILABILITY STATEMENT

Approved for public release; distribution unlimited.

13. SUPPLEMENTARY NOTES
Presented at the 53rd JANNAF Joint Propulsion Meeting (JPM), 2nd Liquid Propulsion Subcommittee (LPS) and Spacecraft Propulsion Subcommittee (SPS), Monterey, CA, 5-8 Dec 2005.

14. ABSTRACT

In order to gain a better understanding of some of the underlying physics associated with the interaction of high-amplitude acoustic waves and a coaxial-jet type injector similar to those used in cryogenic liquid rockets, a non-reacting-flow experimental investigation was conducted under sub-, near-, and supercritical chamber pressures, with and without acoustical excitation. Past research works on this subject have shown both the relevance and importance of geometrical changes in an injector's exit-area and its nearby physical and fluid mechanical processes. On this basis, special attention is paid in collecting spatially-resolved mean temperatures and documenting the aforementioned interactions at the exit of this injector. Short-duration and high-speed digital cameras provided information on the dynamic behavior of this jet under a variety of conditions. Mean and root mean square (RMS) values of the coaxial-jet dark-core length fluctuations were measured from the acquired images via a computer-automated method. It is seen that as the outer-to-inner jet velocity ratio increases, the RMS of the dark-core length fluctuations decreases. It is hypothesized that a connection to rocket instability can be obtained from the data analyzed thus far by way of the magnitude of the RMS values of the dark-core length fluctuations. It is possible that decreases in the fluctuation levels, which were shown here to occur at higher velocity ratios, could weaken a key feedback mechanism for the self-excitation process that is believed to drive the combustion instability in rocket engines. This could offer a possible explanation of the combustion stability improvements experienced in engines under higher outer-to-inner jet velocity ratios. Additional analysis and data acquisition are planned to further investigate this initial finding. Finally, there also appears to be a good correlation between the dark-core length and the outer-to-inner jet momentum flux ratio, but the form of this dependence was found to be different at subcritical pressures than the rest of the chamber conditions (i.e., near- and supercritical cases).

15. SUBJECT TERMS

16. SECURITY CLASSIFICATION OF:			**17. LIMITATION OF ABSTRACT**	**18. NUMBER OF PAGES**	**19a. NAME OF RESPONSIBLE PERSON**
					Dr. Douglas G. Talley
a. REPORT	**b. ABSTRACT**	**c. THIS PAGE**	A	21	**19b. TELEPHONE NUMBER** *(include area code)*
Unclassified	**Unclassified**	**Unclassified**			(661) 275-6174

14. ABSTRACT

In order to gain a better understanding of some of the underlying physics associated with the interaction of high-amplitude acoustic waves and a coaxial-jet type injector similar to those used in cryogenic liquid rockets, a non-reacting-flow experimental investigation was conducted under sub-, near-, and supercritical chamber pressures, with and without acoustical excitation. Past research works on this subject have shown both the relevance and importance of geometrical changes in an injector's exit-area and its nearby physical and fluid mechanical processes. On this basis, special attention is paid in collecting spatially-resolved mean temperatures and documenting the aforementioned interactions at the exit of this injector. Short-duration and high-speed digital cameras provided information on the dynamic behavior of this jet under a variety of conditions. Mean and root mean square (RMS) values of the coaxial-jet dark-core length fluctuations were measured from the acquired images via a computer-automated method. It is seen that as the outer-to-inner jet velocity ratio increases, the RMS of the dark-core length fluctuations decreases. It is hypothesized that a connection to rocket instability can be obtained from the data analyzed thus far by way of the magnitude of the RMS values of the dark-core length fluctuations. It is possible that decreases in the fluctuation levels, which were shown here to occur at higher velocity ratios, could weaken a key feedback mechanism for the self-excitation process that is believed to drive the combustion instability in rocket engines. This could offer a possible explanation of the combustion stability improvements experienced in engines under higher outer-to-inner jet velocity ratios. Additional analysis and data acquisition are planned to further investigate this initial finding. Finally, there also appears to be a good correlation between the dark-core length and the outer-to-inner jet momentum flux ratio, but the form of this dependence was found to be different at subcritical pressures than the rest of the chamber conditions (i.e., near- and supercritical cases).

15. SUBJECT TERMS

16. SECURITY CLASSIFICATION OF:			17. LIMITATION OF ABSTRACT	18. NUMBER OF PAGES	19a. NAME OF RESPONSIBLE PERSON
a. REPORT	b. ABSTRACT	c. THIS PAGE			
unclassified	**unclassified**	**unclassified**		**21**	

PREPRINT

EXPERIMENTS ON A COAXIAL INJECTOR UNDER AN EXTERNALLY-FORCED TRANSVERSE ACOUSTIC FIELD

D. W. Davis and B. Chehroudi
ERC, Inc.
Edwards AFB, CA
and
D. G. Talley
AFRL/PRSA
Edwards AFB, CA

ABSTRACT

In order to gain a better understanding of some of the underlying physics associated with the interaction of high-amplitude acoustic waves and a coaxial-jet type injector similar to those used in cryogenic liquid rockets, a non-reacting-flow experimental investigation was conducted under sub-, near-, and supercritical chamber pressures, with and without acoustical excitation. Past research works on this subject have shown both the relevance and importance of geometrical changes in an injector's exit-area and its nearby physical and fluid mechanical processes. On this basis, special attention is paid in collecting spatially-resolved mean temperatures and documenting the aforementioned interactions at the exit of this injector. Short-duration and high-speed digital cameras provided information on the dynamic behavior of this jet under a variety of conditions. Mean and root mean square (RMS) values of the coaxial-jet dark-core length fluctuations were measured from the acquired images via a computer-automated method. It is seen that as the outer-to-inner jet velocity ratio increases, the RMS of the dark-core length fluctuations decreases. It is hypothesized that a connection to rocket instability can be obtained from the data analyzed thus far by way of the magnitude of the RMS values of the dark-core length fluctuations. It is possible that decreases in the fluctuation levels, which were shown here to occur at higher velocity ratios, could weaken a key feedback mechanism for the self-excitation process that is believed to drive the combustion instability in rocket engines. This could offer a possible explanation of the combustion stability improvements experienced in engines under higher outer-to-inner jet velocity ratios. Additional analysis and data acquisition are planned to further investigate this initial finding. Finally, there also appears to be a good correlation between the dark-core length and the outer-to-inner jet momentum flux ratio, but the form of this dependence was found to be different at subcritical pressures than the rest of the chamber conditions (i.e., near- and supercritical cases).

INTRODUCTION

Most, if not all, liquid rocket engines (LRE) experienced a problem with combustion instability during the development phase. The combustion instabilities span from low-frequency, which is a feed-system coupled instability, to high-frequency acoustic instabilities, which depends on the acoustic modes of the chamber. As a consequence, the resulting high-amplitude pressure oscillations can damage the injection and combustion chamber hardware, causing catastrophic failure of the engine. A great deal of work remains to be done to understand the root causes of combustion instability, although two fairly comprehensive treatises on this subject, such as those compiled by Harrje and Reardon[1] and Yang and Anderson[2], have been published.

Many fundamental questions remain to be answered regarding the physical behavior of the propellant jets and other phenomena governing the combustion instability. One such

question is how the fuel and oxidizer jets change behavior during an unstable combustion event. One early study by Heidmann[3] investigated the behavior of liquid oxygen (LOX) jets during a

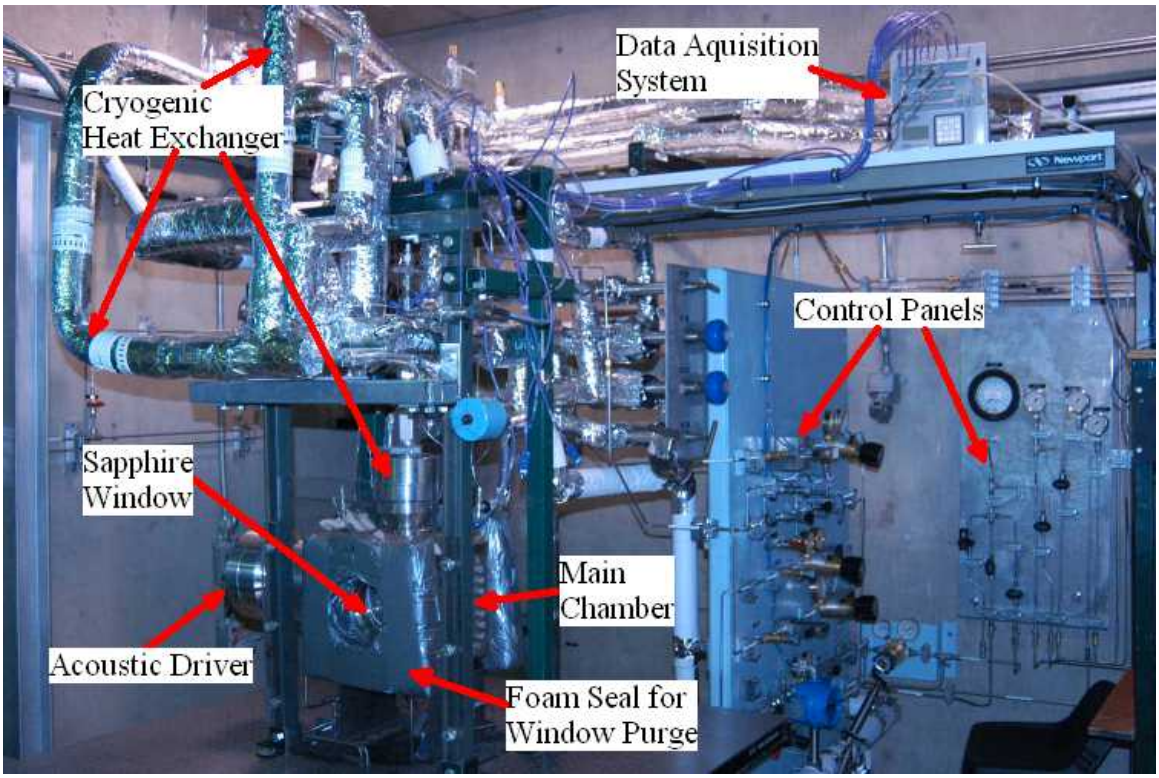

Figure 1. AFRL Supercritical Cold Flow Facility.

period when combustion instability was induced. Hydrogen was introduced into the combustor in a diffuse manner near the LOX jets, making it quite similar to a shear-coaxial injector used in many liquid rocket engines. The LOX jet contracted, once the combustor became unstable. Similar observations were made by Miesse[4] and Buffum and Williams[5] under cold flow conditions when a single round jet was excited with an externally-forced acoustic field.

Mixing of the propellant streams, if not controlling, is at least intimately related to the combustion process. To accomplish combustion in a chamber a given chamber size is required to mix and burn the propellants. With a desire to make smaller combustors possessing high efficiencies, while achieving proper thermal management to prevent burnout of the injection hardware, the need for detailed knowledge of the mixing process becomes critical. To a first order approximation, one measure of the mixing process is the so-called liquid-core length, which has been extensively studied by many researchers in the past.[6-24] A compilation of the experimental core-length correlations, semi-empirical theories, and other data for shear coaxial injector studies involving core length are summarized in Table 1 in the appendix. Although the intent of Table 1 is to compile a comprehensive list of papers reporting the core length of different shear-coaxial jets, it is possible that omissions may have occurred. Many of the correlations and semi-empirical theories reviewed indicate scaling of the core length with outer-jet to inner-jet velocity ratio (V_r), outer-jet to inner-jet momentum flux ratio (M), density ratio (ρ_o / ρ_i), Reynolds number (Re), and Weber number (We). Supercritical pressures and transcritical temperatures are found in liquid rocket engines. One difficulty with applying these relationships to the conditions that may be found in liquid rocket engines is the predicted core length is very small or zero in magnitude, because one of the parameters in the equation is We and surface tension diminishes greatly or vanishes all together,. Transcritical temperatures means that when the fluid is introduced into the combustion chamber it is initially at subcritical temperature, then is heated to a supercritical temperature. To over come the difficulty of core length prediction associated

large *We*, one group of researchers[15-20], proposed that *M* can be used to describe the scaling of core length for shear-coaxial injectors, and need not include *We* if the *We* is sufficiently high.

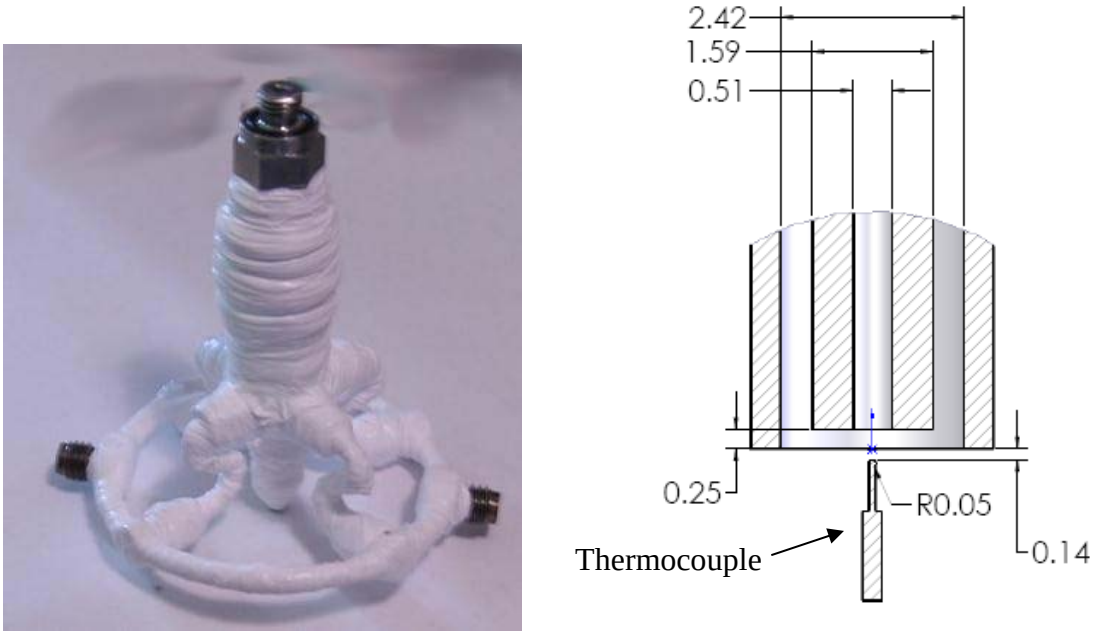

Figure 2. Picture of shear-coaxial injector (left) and cross-section drawing of the injector tip. The thermocouple used to measure exit-plane temperature profiles is shown in the drawing, indicating the relative size and axial position of the measurement.

Chehroudi and co-workers[22-33] have investigated supercritical jet flows at higher Reynolds numbers and turbulent jets of interest to practical applications in propulsion systems. The single round-jet work by Chehroudi et al[25-31] was produced from two different injectors made from 50 mm long sharp-edged tubes with the inner jet diameters of 0.254 mm and 0.508 mm, (L/D of 200 and 100, respectively). They injected pure N2 and O2 into N2, He, Ar, and mixtures of CO and N2 and the arrangement was studied with shadowgraphs and Raman imaging. It was determined that the initial growth rate of a supercritical jet was different from that of a subcritical jet. Furthermore, they quantitatively proved, for the first time, that the initial growth rate of supercritical jet behaved similar to variable-density gas jets.[28] From this observation, a phenomenological model of the initial growth rate based upon time scale arguments was proposed which agreed well with the results acquired under sub- and supercritical pressures.[28] It is also important to note that Chehroudi et al.[29] showed that the growth rate measured from shadowgraphs was about twice as large as the growth rate of the jet measured by Raman imaging of the jet, based on the full width at half maximum (FWHM) jet thickness values. The fractal dimension of the initial region of the jet under sub- and supercritical pressures was also measured for the first time by Chehroudi et al.[26, 29, 31] and compared to liquid and gas jets in a similar fashion to that of the growth rate. A transition from a liquid jet to a gas jet, from sub- to supercritical, in fractal dimension was observed.

EXPERIMENTAL SET-UP

The experimental facility, shown in Fig. 1, has been described in details previously [22-24, 31], and only a brief description will be given here. High-pressure gaseous nitrogen (GN_2) flows into the system, its flow rate measured with Porter Mass Flow meters, and controlled with micrometer needle valves. Temperature conditioning is accomplished by passing the GN_2 through a shell and tube type heat exchanger using liquid nitrogen (LN_2) to cool the GN_2. The nitrogen flows into both the inner and outer tubes. Temperature of the flow to the inner round jet

of the shear-coaxial injector is considerably lower than that of the outer annular jet, reaching the liquid state. However, the outer jet is cooled well below the room temperature, but is still in gaseous state. The chamber is pressurized with GN_2 at ambient temperature. For reference, the critical pressure and temperature of N_2 is 3.4 MPa and 126.2 K, respectively. The pressure inside the main chamber is maintained by adjusting the outlet flow rate using a triplet of valves to provide an optimum level of control.

The test article consists of a chamber within a chamber. The main, external, chamber is used to create a pressurized environment and is fitted with two sapphire windows for observation of the jet behavior. The smaller, internal chamber, acting as an acoustic resonator cavity, is used to keep the amplitude of the acoustic driver (attached at one end) high in the vicinity of the jet. The Piezo Siren acoustic driver, developed by Hersch Acoustical, is capable of producing amplitudes in an impedance tube of up to 180dB at pressures up to 14 MPa. To obtain sufficiently high amplitudes, the driver must resonate the normal modes of the inner chamber. Therefore, the frequency at which the effects are studied is limited to the first two modes of the inner chamber, being about 3 kHz and 5.25 kHz, respectively. The frequency shifts slightly depending on the chamber fluid, temperature, and pressure. The resulting wave length is much larger than the diameter of the jet. The injector is positioned at a pressure node (a velocity anti-node) to produce maximum velocity fluctuations near the jet.

The shear coaxial injector used in this work (see Fig. 2) is based on the well-characterized design of the single-jet injector used in all previous studies[24-30] in this apparatus. The center-post made from a stainless steel tube with an I.D. (D_1) of 0.51 mm (0.020”) and an O.D. (D_2) of 1.59 mm (0.063”) with a length of 50.8 mm (2.00”) used to produce the inner jet. The resulting length to I.D. ratio is 100, which is sufficient to ensure a fully-developed turbulent pipe flow conditions at the exit. The outer stainless steel tube creating the annular passage had an I.D. (D_3) of 2.42 mm (0.095”) and an O.D. (D_4) of 3.18 mm (0.125”) used to produce the outer annular jet. The resulting mean gap width of the annular passage, the hydraulic radius, is 0.415 mm (0.016”), measured from an image taken at the exit of the injector. The injector has a small bias of 8% of the mean gap width. The recess of the inner tube was 0.5 D_1, 0.25 mm (0.010”) from the end of the outer tube.

Because of the proximity of the experimental conditions to the critical point of nitrogen, accurate measurements of temperature were necessary to obtain reliable estimates of density and other quantities computed from the density. Radial temperature profiles were measured using a type E exposed bead thermocouple that was traversed through the jet measuring mean temperature. At cryogenic temperatures, the accuracy of thermocouples is not reliable. However, due to the small size of the system of interest, a Pt-RTD was not feasible. Therefore, it was necessary to calibrate the individual thermocouples against a precision Pt-RTD. The temperature profiles and the details of the calibration were reported elsewhere.[22,23]

Shadowgraph images of the jet were taken using either a PixelFly CCD camera or a Phantom v5.1 or v7.1 CMOS camera. The advantage that the CMOS cameras presented was the ability to produce high-speed movies of the jet for a period lasting up to several seconds. The framing rate for the movies in this work was 18.00 kHz.

RESULTS AND DISCUSSION

ACOUSTIC WAVE INTERACTION WITH SHEAR-COAXIAL JET

High speed movies of the jet present a large amount of information about the flow being studied. A sample of ten consecutive images at sub- (rows one and two from top), near- (rows three and four), and supercritical (rows five and six) chamber pressures are shown in Fig. 3. Rows one, three, and five are for when the acoustic driver is off and the remaining ones are when it is activated at ~ 3kHz. The evolution of the jet in time is from left to right in Fig. 3, with the time

between frames being 55.6 μs. Prominent in all the visualizations of the jet is existence of a dark central region which we refer to as a dark core. The dark core under the unexcited subcritical

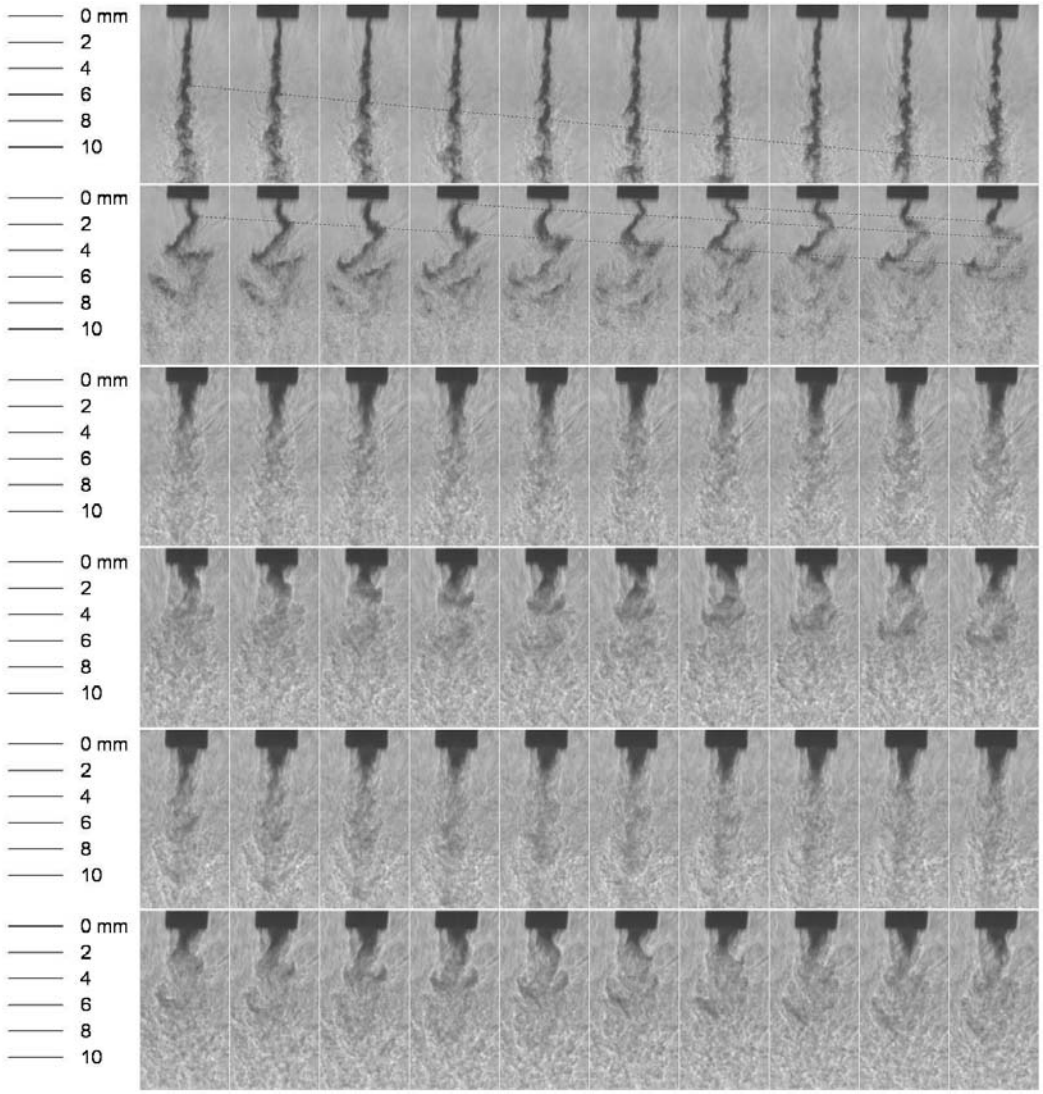

Figure 3. Consecutive frames from high-speed shadowgraph images with the acoustic driver turned off and on at ~3kHz. Time increases from left to right with an interval of 55.6 μs between frames. The first two rows are at a subcritical chamber pressure (~ 1.5 MPa), the third and fourth rows are at a near-critical chamber pressure (~ 3.5 MPa), and the fifth and sixth rows are at a supercritical chamber pressure (~ 4.9 MPa). The acoustic driver is turned off for the first, third, and fifth rows and on for the second, fourth, and sixth at ~ 3 kHz. The light gray lines in the first and second rows connect fluid structure as they evolve in time.

pressures (Fig. 3, row one) can be approximated as a cylindrical-like structure with unstable surface waves of low amplitude. However, upon increasing the pressure to near- and supercritical pressures (rows three and five) this structure changes to a more conical shape. The conical structure of the dark core has been reported before for single-phase coaxial jets by Lasheras and Hopfinger.[20] As clearly demonstrated in images of Fig. 3 and the other visualizations obtained in this work (not shown here), the conical-shape structure was not observed under two-phase conditions (i.e. subcritical chamber pressure).

Excitation of the jet with acoustic driver yields significantly different behavior of the dark core compared to that of the unexcited one. The strongest effect is observed under subcritical pressures. The cause of this effect is not completely clear at this time. However, it is believed to be as a result of the operation of the acoustic driver at a constant power level at the three

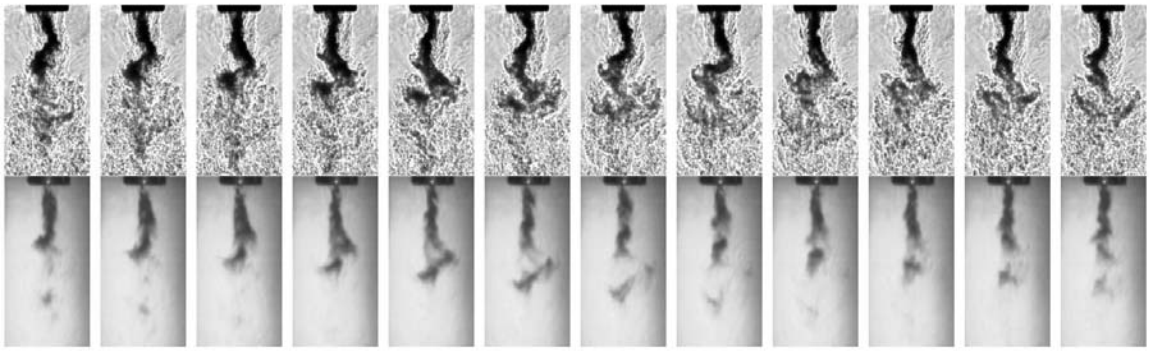

Figure 4. Simultaneous images of the acoustically-excited jet under subcritical conditions viewed from the direction perpendicular (top row) and parallel (bottom row) to the acoustic velocity. The top row was back-lit, but due to geometrical limitations of the apparatus it was necessary to illuminate the jet from the front in the bottom row. Time increases from left to right. The framing rate of the two cameras was 18 kHz and the driving frequency was 3 kHz, approximately two cycles of the acoustic driver are represented in these images.

pressure levels tested. This is a limitation of the current equipment. As the chamber pressure is increased the density of the chamber fluid increases also. Therefore, there is more mass for the driver to move and oscillate, thus the amplitude of the velocity fluctuations is reduced at higher pressures. This remains to be verified, as more data is acquired and analyzed.

The direction of the acoustically-induced velocity fluctuations is horizontal (towards left and right) in images of Fig. 3. The core of the jet forms large-scale sinusoidal structures as a result of this imposed velocity field oscillations. To investigate the modal behavior of the jet, two Phantom CMOS cameras were synchronized and the jet imaged both perpendicular and parallel to the acoustic velocity fluctuations. Twelve consecutive images of the jet (approximately two cycles of the acoustic oscillation period), viewed perpendicular (top row) and parallel (bottom row) to the acoustic velocity field, are shown in Fig.4. The large-scale oscillations of the dark core are principally in the direction of the acoustic velocity. Some three-dimensional movement of the core does occur, but these motions do not occur in a periodic manner, as do the jet oscillations in the direction of the acoustic velocity. The large-scale oscillations of the dark core seen in the top row of Fig. 4 are periodic and correspond to the driving frequency, as tested at the two resonance modes of the chamber (~ 3 and 5.2 kHz). It appears from these movies, as fluid leaves the injector tip the momentum from the acoustically-induced motion causes a transverse displacement pushing the core of the jet into the higher speed annular jet. The dense fluid from the core experiences acceleration in the axial direction, which is caused by the high speed annular jet. Upon reversal of the acoustic field, the dense fluid, initially from the core now in higher speed annular flow, appears to maintain the transverse component of momentum imparted to it upon leaving the injector and the dense fluid particle does not reverse direction. The dense fluid parcel then slows (both in the axial and transverse directions) as it arrives at the shear layer

between the outer jet and the chamber fluid farther downstream, where a “cusp-shaped” structure is formed from the dense fluid originating in the core of the jet . Subsequent mixing and heat transfer from the outer jet to the inner jet core fluid ultimately causes the fluid parcel to be indistinguishable from the outer jet fluid.

DARK CORE LENGTH MEASUREMENT

As indicated in Table 1 (in the appendix), many techniques have been employed to measure the core length of a coaxial jet, ranging from Pitot tube measurements to analysis of images. The measurements in this work are taken from a great number of images in a systematic fashion to provide repeatable results. In the past, final results have been reported on as few as four number of images.[10]

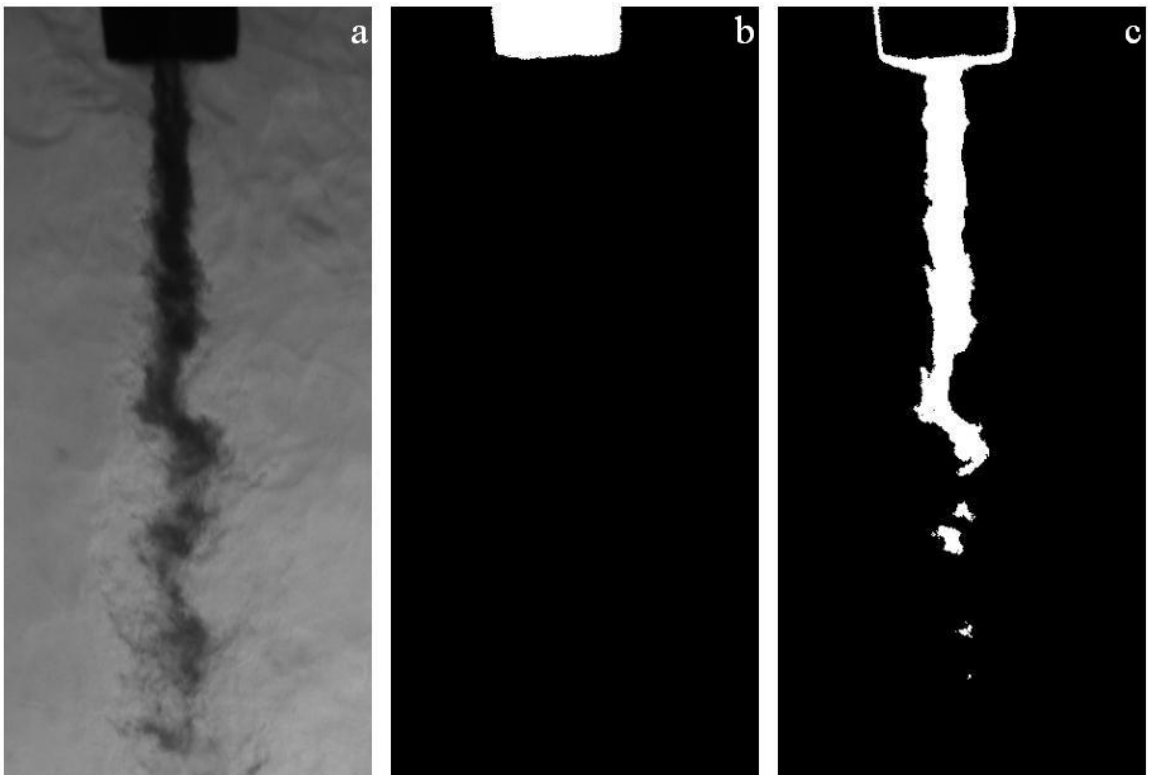

Figure 5. The image of (a) coaxial jet as captured, (b) threshold applied for injector, (c) threshold applied for dark core.

The algorithm for measuring the dark-core length starts with an individual image, such as Fig. 5(a). From this image, the image histogram, that is, number of pixels vs. gray level, is computed, as shown in Fig.6 for the image shown in Fig. 5(a). The first peak, located within the gray-scale values below that of the dashed (vertical) line level denotes those corresponding to the injector tip. Ideally, the

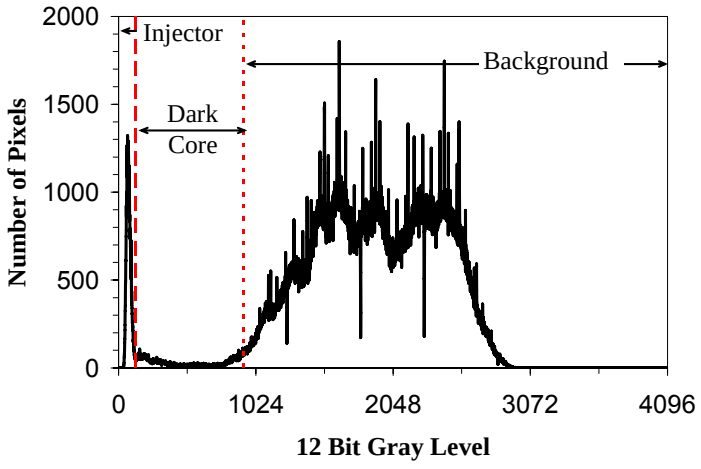

Figure 6. Histogram of image in Fig. 3a.

injector tip should be completely opaque (corresponding to a zero gray-scale value), but due to internal reflections within the chamber this peak shifts slightly off the zero value. The gray levels defining the dark core, ends with the rise of large broad peak on the right, denoting the background, see the dotted vertical line in Fig. 6. This dotted-line gray level is determined by a non-linear curve fitting technique using a Gaussian function to fit to the region of the histogram in the vicinity of the rise of the background information. The slope of this fitted curve is then calculated by differentiation and the gray level at which the slope of the histogram exceeds e^{-1} is determined to be the end of the gray levels defining the dark core, which corresponding to the dotted line in Fig. 6.. A binary threshold is then applied to the image between the gray levels indicated by the injector tip (Fig. 5(b)) and the rise of the background information. The resulting image is shown in Fig. 5(c). Such images are then used to measure the axial length of what we refer to as the "dark core" from the injector exit to the end of the interconnected white region seen in this figure. Results from this technique compared well with those when visual judgments were used, see Davis et al.[23]

It should be mentioned that confusion exists in the literature especially when vague definitions are used when defining a core length. The terms potential-core, potential-cone, intact-length, intact-liquid-length, and breakup-length are all used along with various measurement techniques (see Table 1). To be clear, and remove any possible ambiguity from the data, dark-core length is defined here as the connected dark fluid region between the injector exit area and the first break in the core as defined by the adaptive thresholding procedure outlined above.

INFLUENCE OF VELOCITY RATIO ON THE DARK CORE

Velocity ratio (outer-to-inner jet) has been a design parameter for shear-coaxial injectors, particularly, as a criterion to ensure the stable operation of LREs. For LOX/H_2 engines. the design rule-of-thumb has been to keep the velocity ratio greater than about 10 to keep the engine stable.[34] Although experimental data suggests this criterion, no physical explanation has been provided. One method to rate a LRE for combustion instability is temperature ramping, which is accomplished by lowering the temperature of the H_2 while maintaining mass flow rate at a constant value. The lower the H_2 temperature is at the onset of the measured combustion instability, the greater the stability margin of that particular LRE. Note that as the H_2 temperature is lowered at a constant mass flow rate, the velocity ratio is also lowered.

To determine the effects of the outer-jet temperature (which is GN_2 in this work) on the coaxial jet, two nominal temperatures were studied (called high and low). The averaged dark-core lengths are shown in Figs. 7(a) and 8(a) as a function of velocity ratio (V_r). The RMS of the variations of the dark core length is also shown in Figs. 7(b) and 8(b). Figures 7 and 8 present results for conditions when the external acoustic field is turned on and off for both nominal high and low outer-jet temperatures of ~190 K and ~140 K, respectively. According to Eroglu et al.[10], the average of the length measured from individual images of a set can be regarded as the time averaged value. It should be noted that, for each operating condition in this work, length measurements were also made from an averaged image of a set. In general, the length measured from the averaged image is slightly shorter than the average of the individual dark-core values calculated in a given set.

Evident in Figs. 7(a) and 8(a) is the fact that the length of the dark core decreases as the chamber pressure is increased. The dark core provides an indication of high-density regions of the flow. At a constant chamber pressure, as V_r is increased, the length of the dark core decreases and appears to approach a constant value. In a mean sense, when the dark core feels the imposed external acoustic field, its length is shorter than or equal to the that when the acoustic driver is turned off. Under the near- and supercritical chamber pressures, as the V_r increases, the difference between the lengths of the dark core, measured with and without the acoustic field, diminishes. The RMS values of the dark-core length fluctuations, shown in Figs. 7 (b) and 8(b), exhibit somewhat similar trends to those seen with the mean values. It is known that

for a liquid-fueled rocket, atomization and breakup processes, interactions between the propellant jets, droplet formation, and vaporization are all affected by the pressure and, particularly, velocity fluctuations. Also, for any chemically-reacting system, the rate at which energy is released is sensitive to the rate of change of temperature, density, pressure, and, of course, mixture ratio. It is then quite intuitive to relate, in some form, the RMS values of the dark-core length fluctuations to mixture ratio variations. On the other hand, a low RMS value can be interpreted as the jet's inherent steadiness and vice versa. Examination of Figs. 7b and 8b clearly shows that this property is drastically reduced as the velocity ratio is increased. Although these results are for a single injector, it is then quite possible that the observed improvement in combustion stability at higher values of velocity ratio is a result of the inability of the jet to generate large mass flow rate

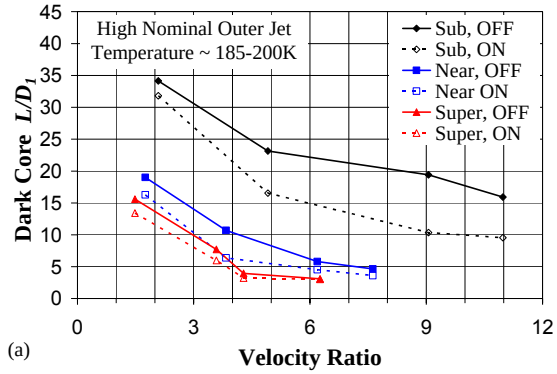

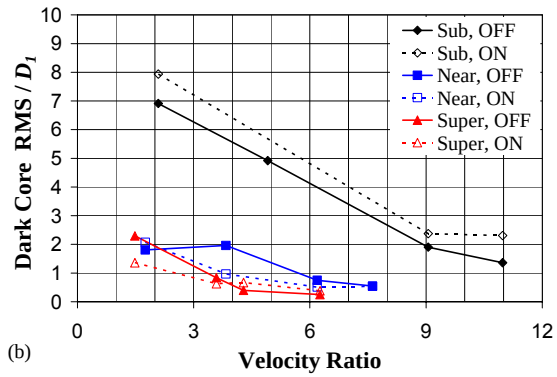

Figure 7. Plot of the averaged dark-core length (a) and the RMS of the length variations (b) normalized by the inner diameter. The solid symbols and lines represent the data for when the acoustic driver is *off*, and the hollow symbols and dotted lines show the data when the acoustic driver was operated at ~ 3kHz. The diamond, square, and up-triangle symbols are sub-, near and supercritical chamber pressures, respectively. All cases are for the higher nominal outer-jet temperature of ~190 K. In the inset the words sub, near, and super refer to subcritical, nearcritical, and supercritical pressure respectively, and the words OFF and ON refer to the acoustic driver being off and on at ~3kHz, respectively.

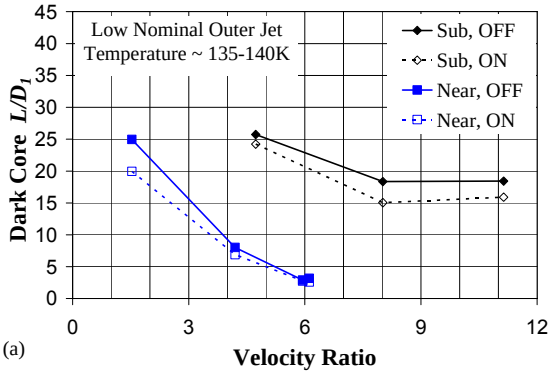

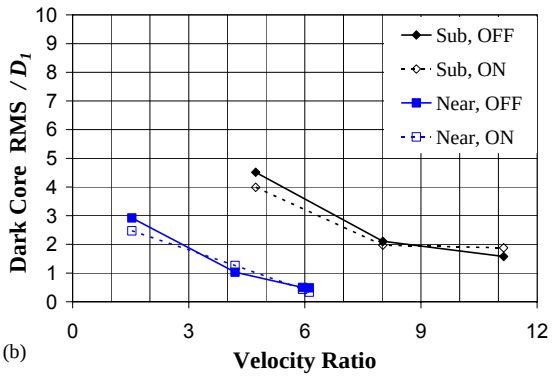

Figure 8. Plot of the averaged dark-core length (a) and the RMS of the length variations (b) normalized by the inner diameter. The solid symbols and lines represent data for when the acoustic driver off, and the hollow symbols and dotted lines show results when the acoustic driver is operated at ~ 3kHz. The diamond and square symbols are for sub- and nearcritical chamber pressures, respectively. All cases are for the lower nominal outer-jet temperature of ~140 K. In the inset the words sub and near refer to subcritical and nearcritical pressure respectively, and the words OFF and ON refer to the acoustic driver being off and on at ~3kHz, respectively.

fluctuations under these conditions, weakening a key feedback line for the self-excitation process. In temperature ramping exercises for stability rating of LOX/H2 engines, the mass flow rate is usually maintained at a constant value.[34] Therefore, as the temperature of the H_2 is decreased during a ramping episode, the H_2 becomes more dense, which decreases the injector velocity ratio. The RMS plots shown here suggest that such a decline in this ratio amplifies the jet's inherent unsteadiness, providing a possible explanation for the engine's eventual arrival into an unstable zone as a temperature ramping test proceeds.

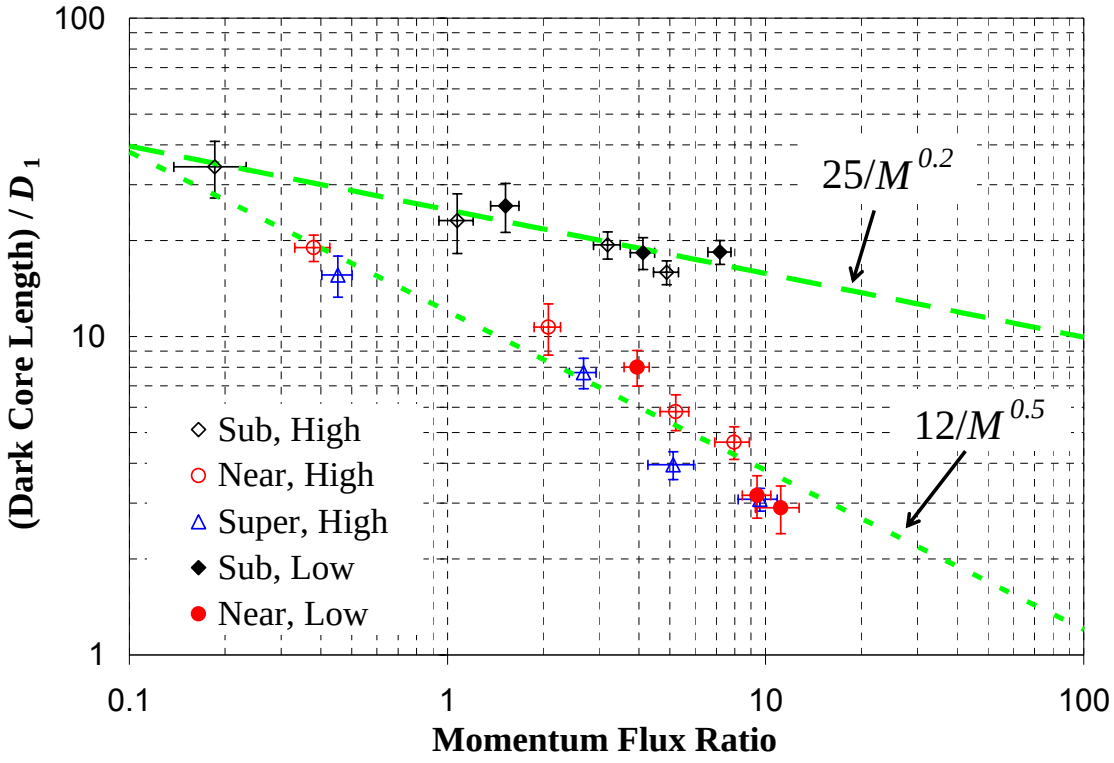

Figure 9. Dark-core length versus momentum flux ratio. The diamond, circle, and up-triangle symbols represent sub-, near-, and supercritical chamber pressure, respectively. The hollow symbols are at a high outer-jet temperature (~190 K) and solid symbols are at a low outer-jet temperature. The dashed line is $25/M^{0.2}$ and the dotted line is $12/M^{0.5}$.

SCALING OF THE DARK CORE

As mentioned above, the core length has been scaled with many parameters. In some work, *We* and *Re* numbers were used to represent velocity values in nondimensionalized forms, as physical parameters, such as surface tension and viscosity, were not varied. In other work, based on single-phase results, velocity ratio (V_r) or momentum flux ratio (M) were considered as the scaling parameters. The semi-empirical theory of Rehab et al.[17] which is based on an entrainment velocity of the inner jet into the outer jet and a resulting mass balance on the core of the jet, produces an equation suggesting that the length of the core scales with $M^{-0.5}$. This equation was then quantitatively compared to single-phase shear-coaxial jet data, often with equal densities.[16-18] Note that for (inner and outer) jets of equal densities, $M^{-0.5}$ reduces to V_r. The same dependence on M was also reported qualitatively for single-phase shear-coaxial jets of

different densities by Favre-Marinet and Samano-Shettini.[21] Additionally, Lasheras et al.[19] stated applicability of the same $M^{-0.5}$ dependence form for two-phase shear-coaxial jets. However, they were unable to make core length measurements from their images.

A plot of the measured dark-core length values, of this work, versus momentum flux ratio is shown in Fig. 9. A clear distinction between the subcritical dark-core length (diamond symbols) and that for the near- and supercritical chamber pressures are seen. Subcritical data indicates a much longer length than the supercritical pressure for a given momentum flux ratio.. It should be noted that the near-critical pressure data is slightly supercritical, and both the near- and supercritical pressure conditions produce a single-phase coaxial jet. The dashed line in Fig. 9 is a least-square curve fit to the subcritical data, and the dotted line is a least squares curve fit to the near- and supercritical data. As indicated by the equations on Fig. 9, the single-phase

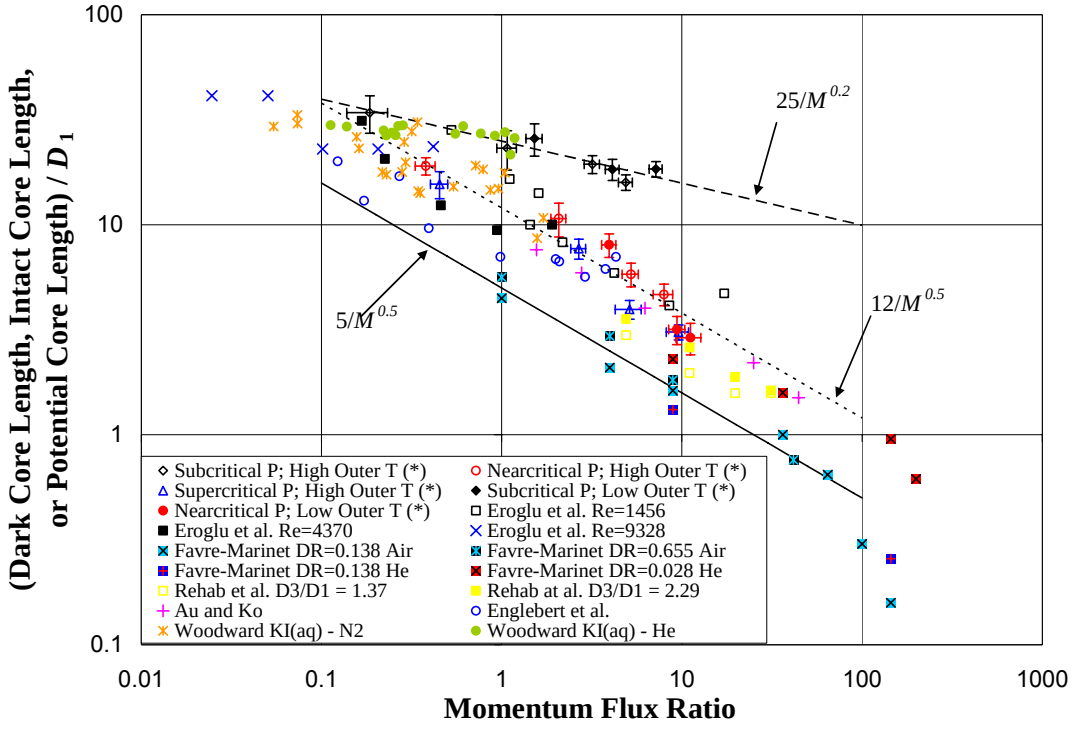

Figure 10. Comparison of present dark-core length with all the core-length data available in the literature vs. momentum flux ratio. Of the data from the literature, Eroglu et al, Englebert et al., and Woodward are two-phase flows and the rest are single phase. The references for the data are found in Table 1.

(i.e., near- and supercritical pressures), data have the same $M^{-0.5}$ dependence form as reported by others.[16-18, 21] However, the two-phase subcritical data has a weaker dependence, $M^{-0.2}$, than the single-phase dark-core length. Other quantitative differences between subcritical and supercritical have been reported before. For single round jets, Chehroudi[28,29, 31] and co-workers found that under supercritical pressures the spreading rate and fractal dimension values were the same as those for a gaseous jet injected into a gaseous ambient with different densities (i.e., variable-density, single-phase, gaseous jet). This is a similar observation but for the dark-core length. Under supercritical pressures, our coaxial jet scales with $M^{-0.5}$. Therefore, it appears that this form of the dependency to M is not only valid for gas-gas shear-coaxial jets, but as any single-phase shear-coaxial jet, such as the system where the original dependence f $M^{-0.5}$ was found from the water-water work of Rehab et al.[16,17]

Figure 10 was constructed with the objective of comparing the dark-core length with all of the available data that exists in the literature for the potential-core length, intact-core length, and breakup-length. Figure 10 represents all of the available data in the literature concerning core length spanning 5 orders of magnitude in momentum flux ratio. Also, note that as M approaches zero, one reaches a limit defining a single round jet configuration because the outer velocity becomes zero. From data in Fig 10, it seem that for $M < 1$, data points converge and approach the core length range expected for single round jets reported by Oschwald et al[33]. The single-phase data presented in Fig. 10 follows the dependence of $L/D_1 = A\, M^{-0.5}$, where the constant A is between 5 and 12. At $M > 100$, the data points of Favre-Marinet and Samano-Shettini[21] exhibit a recirculation bubble at the end of the core, and thus the core length decreases. The injectors used to produce the two-phase coaxial jets of Eroglu et al.[10] and Englebert et al.[12] have much larger outer jet gap widths (see Table 1) than what is typical of rocket type injectors. Additionally, the apparatus of Eroglu et al[10] , reported in Farago and Chigier[35] , does not produce fully-turbulent inner jet until when $Re > 10^4$. The lack of a fully-turbulent inner jet and the significant differences between their injector and shear-coaxial ones used in rockets could be the reasons the core length measured by Eroglu et al[10] is shorter than those observed in our work. Englebert et al.[12] reported that the core length scaled with $M^{-0.3}$. The core length by Woodward[11] for the water potassium iodide solution with helium, however, obeys very nearly the trends for the subcritical data points (i.e., $25M^{-0.2}$). Considering that momentum flux ratios near 10 are of importance for LRE, to the best of the authors' knowledge, the data for the subcritical (two-phase) case is the only reported information in the neighborhood of the $M = 10$.

SUMMARY AND CONCLUSIONS

A non-reacting flow study of a cryogenic shear-coaxial injector was conducted at pressures spanning subcritical to supercritical values. The flow from the inner jet of the coaxial injector was liquid nitrogen (or liquid-like, if at supercritical pressures) and cold gaseous nitrogen flowed from the outer annular jet, both injected into a chamber pressurized with nitrogen at room temperature. The resulting coaxial jet was imaged with a camera framing at a rate of up to 18 kHz. The jet was excited with a high-amplitude acoustic driver, with the jet located at a velocity anti-node (pressure node). The following conclusions are offered:

1. The high-amplitude acoustic wave alters the behavior of the shear-coaxial jet. The resulting structure of the jet exhibits a periodic shape corresponding to the transverse-velocity field created by the acoustic waves. The periodic oscillation of the core of the jet is predominately in the direction of the transverse acoustic velocity. No helical mode of for the jet was observed.
2. The quantitative behavior of the dark-core length for the coaxial jet at near- and supercritical pressure follows similar momentum flux ratio (M) dependency reported for the single-phase shear-coaxial jets (i.e., $12M^{-0.5}$). The dark-core length for the subcritical pressures, however, scales with $M^{-0.2}$.
3. Within a range of momentum flux ratios in between 1 and 10, the dark-core lengths for the coaxial jet under the subcritical (two-phase) ambient pressure used here appear longer than those measured at the supercritical (single-phase) condition. Considering the upper bound of this range represents relevant values for liquid rocket engines, subcritical data define a new regime which was not reported previously.

NOMENCLATURE

A = area
B = a constant on the order of 10^{-3}
C = 0.5 constant
c = a constant
D = diameter

E_R = energy ratio $(\rho_o U_o^3 A_o)/((\rho_i U_i^3 A_i)$
L = dark-core length, potential core, intact core, or breakup length
$Lpost$ = length of undisturbed entrance length of inner tube of the coaxial injector
R = radius
r = correlation parameter dependent on gas properties
Re = Reynolds Number $(\rho U D)/\mu$
M = momentum flux ratio of the outer jet to inner jet $(\rho_o U_o^2)/((\rho_i U_i^2)$
M_R = momentum ratio $(\rho_o U_o^2 A_o)/((\rho_i U_i^2 A_i)$
U = velocity
V_r = velocity ratio of the outer jet to inner jet
We = Weber number $(\rho_o (U_o - U_i)^2 D_1 / \sigma$
Z = Ohnesorge Number

GREEK SYMBOLS

α = 0.17 constant
μ = viscosity
ρ = density
σ = surface tension

SUBSCRIPTS

1, 2, 3, 4 the four diameters defining the edges of a coaxial injector from innermost to outermost

i inner

o outer

ACKNOWLEDGMENTS

The authors would like to acknowledge Mr. Mike Griggs for his valuable contributions in the improvements to the experimental facility. Lt. Matthew Raskie, Lt. Jason Szuminski, Mr. Earl Thomas, Mr. Randy Harvey, Mr. David Hill, and Mr. Mark Wilson are thanked for their efforts. Additionally, Ms. Jennie Paton is thanked for making literature available in a timely manner. A great appreciation is extended to Mr. Steven Martin for loaning the authors one of the Phantom Cameras. A special gratitude is expressed to M. Favre-Marinet, E. B. Camano Schettini, and R. D. Woodward for providing us with their core length data in tabular form. The first author would like to thank his thesis advisor, Dr. R. J. Santoro, for many helpful discussions permitting his thesis work to be performed off-campus at AFRL. This work is sponsored by the Air Force Office of Scientific Research under Dr. Mitat Birkan, program manager.

REFERENCES

1. Harrje, D. T. and Reardon, F. H. (eds.), ***Liquid Propellant Rocket Combustion Instability***, NASA SP-194, 1972.
2. Yang, V. and Anderson, W. (eds.), ***Liquid Rocket Engine Combustion Instability***, Progress in Astronautics and Aeronautics, AIAA, Washington, DC, 1995.
3. Heidmann, M. F. ***Oxygen Jet Behavior During Combustion Instability in a Two-Dimensional Combustor***, NASA TN D-2725, 1965.
4. Miesse, C. C., "The effect of ambient pressure oscillations on the disintegration and dispersion of a liquid jet", ***Jet Propulsion***, Vol. 25, 1955, pp. 525-530, 534.

5. Buffum, F. G., and Williams, F. A., "Response of turbulent liquid jets to transverse acoustic fields", ***Proceedings of the 1967 Heat Transfer and Fluid Mechanics Institute***, Edited by P. A. Libby, D. B. Olfe, and C. W. Van Atta, 1967, pp. 247-276.
6. Forstall, W., and Shapiro, A. H., "Momentum and Mass Transfer in Coaxial Gas Jets," ***J. Applied Mechanics***, Trans. ASME, Vol. 72, 1950, pp. 399-408.
7. Chigier, N. A., and Beer, J. M., "The Flow Region Near the Nozzle in Double Concentric Jets," ***J. of Basic Engineering***, Trans. ASME, Vol. 4, 1964, pp. 797-804.
8. Champagne, F. H., and Wygnanski, I. J., "An experimental Investigation of Coaxial Turbulent Jets," ***International Journal of Heat and Mass Transfer***, Vol. 14, 1971, pp. 1445-1464.
9. Au, H., and Ko, N. W. M., "Coaxial Jets of Different Mean Velocity Ratios, Part 2," ***Journal of Sound and Vibration***, Vol.116, No. 3, 1987, pp. 427-443.
10. Eroglu, H., Chigier, N., and Farago, Z., "Coaxial Atomizer Intact Lengths," ***Physics of Fluids A***, Vol. 3, No. 2, Jan. 1991, pp. 303-308.
11. Woodward, R. D., ***Primary Atomization of Liquid Jets Issuing from Rocket Engine Coaxial Injectors***, Ph.D. Thesis, Mechanical Engineering Dept., The Pennsylvania State University, University Park, PA, 1993.
12. Englebert, C., Hardalupas, Y., and Whitlaw, J. H., "Breakup Phenomena in Coaxial Air-Blast Atomizers," ***Proc. R. Soc***., Vol. 451, London, 1995, pp. 189-229.
13. Carreau, J. L, Porcheron, E.., LeVisage, D., Prevost, L., and Roger, F., "Liquid Core Characterization of Coaxial Liquid Oxygen/Inert Gas Jets," ***Int. J. of Fluid Mech. Research***, Vol. 24, Nos. 4-6, 1997, pp.498-507.
14. Porcheron, E.., Carreau, J. L., Prevost, L., LeVisage, D., and Roger, F., "Effect of Density on Coaxial Liquid Jet Atomization," ***Atomization and Sprays***, Vol. 12, 2002, pp. 209-227.
15. Villermaux, E., Rehab, H., and Hopfinger, E. J., "Breakup Regimes and Self-Sustained Pulsations in Coaxial Jets," ***Meccanica***, Vol. 29, 1994, pp. 393-401.
16. Rehab, H., Villermaux, E., and Hopfinger, E. J., "Geometrical Effects of Near-Field Flow Structure of Coaxial Jets," ***AIAA Journal***, Vol. 36, No. 5, 1998, pp. 867-869.
17. Rehab, H., Villermaux, E., and Hopfinger, E. J., "Flow Regimes of Large Velocity Ratio Coaxial Jets," ***J. Fluid Mech***., 1997, pp.357-381.
18. Villermaux, E., "Mixing and Spray Formation in Coaxial Jets," ***J. Propulsion and Power***, Vol. 14, No. 5, 1998, pp. 807-817.
19. Lasheras, J. C, Villermaux, E., and Hopfinger, E. J., "Breakup and Atomization of a Round Water Jet by a High Speed annular Air Jet," ***J. Fluid Mech.***, Vol. 357, 1998, pp. 351-379.
20. Lasheras, J. C., and Hopfinger, E. J., "Liquid Jet Instability and Atomization in a Coaxial Gas Stream," ***Annual Rev. Fluid Mech.***,Vol. 32, 2000, pp. 275-308.
21. Favre-Marinet, M., and Camano Schettini, E. B., "The Density Field of Coaxial Jets with Large Velocity Ratio and Large Density Differences," ***International Journal of Heat and Mass Transfer***, Vol. 44, 2001, pp. 1913-1924.
22. Davis, D. W. and Chehroudi, B., "The Effects of Pressure and Acoustic Field on a Cryogenic Coaxial Jet," ***42nd AIAA Aerospace Sciences Meeting & Exhibit***, AIAA, Washington, DC, 5-8 Jan. 2004.
23. Davis, D. W., Chehroudi, B., and Sorensen, I. "Measurements in an Acoustically Driven Coaxial Jet under Supercritical Condition," ***43rd AIAA Aerospace Sciences Meeting & Exhibit***, AIAA, Washington, DC, 10-13 Jan. 2005.
24. Davis, D. W., and Chehroudi, B., "Measurements of an Acoustically Driven Coaxial Jet under Sub-, Near-, and Supercritical Conditions," ***J. of Propulsion and Power***, 2005 (submitted).
25. Chehroudi, B., Talley, D., and Coy, E. B., "Initial Growth Rate and Visual Characteristics of a Round Jet into a Sub- to Supercritical Environment of Relevance to Rocket, Gas turbine, and Diesel Engines," ***37th AIAA Aerospace Science Meeting and Exhibit***, AIAA, Washington, DC, 11-14 Jan. 1999.
26. Chehroudi, B., Talley, D. G., and Coy, E. B., "Fractal Geometry and Growth Rate Changes of Cryogenic Jets near the Critical Point," ***35th AIAA/ASME/SAE/ASEE Joint Propulsion Conference and Exhibit***, AIAA, Washington, DC, 20-24 Jun. 1999.
27. Chehroudi, B., Cohn, R., Talley, D. G, and Badakhsan, A., "Raman Scattering Measurements in the Initial Region of Sub- and Supercritical Jets," ***36th***

AIAA/ASME/SAE/ASEE Joint Propulsion Conference and Exhibit, AIAA, Washington, DC, 17-19 Jul. 2000.
28. Chehroudi, B., Talley, D. G., and Coy, E. B. "Visual Characteristics and Initial Growth Rates of Round Cryogenic Jets at Subcritical and Supercritical Pressures," ***Physics of Fluids***, Vol.4, No. 2, Feb. 2002. pp. 850-861.
29. Chehroudi, B., Cohn, R., and Talley, D. G., "Cryogenic Shear Layers: Experiments and Initial Growth Rates of Round Cryogenic Jets at Subcritical and Supercritical Pressures," ***International Journal of Heat and Fluid Flow***, Vol. 23, 2002, pp. 554-563.
30. Chehroudi, B., and Talley, D. G., "Interaction of Acoustic Waves with a Cryogenic Nitrogen Jet at Sub- and Supercritical Pressures," ***40th AIAA Aerospace Meeting and Exhibit***, AIAA, Washington, DC, 14-17 Jan. 2002.
31. Chehroudi, B. and Talley, D., "Fractal Geometry of a Cryogenic Nitrogen Round Jet Injected into Sub- and Super-critical Conditions", ***Atomization and Sprays***, Vol. 14, 2004, pp. 81-91.
32. Chehroudi, B., Davis, D. W., and Talley, D. G., "Initial Results from A Cryogenic Coaxial Injector In An Acoustic Field," ***41st AIAA Aerospace Sciences Meeting & Exhibit***, AIAA, Washington, DC, 6-9 Jan. 2003.
33. Oschwald, M., Smith, J. J., Branam, R., Hussong, J., Schik, A., Chehroudi, B., and Talley, D. G., "Injection of Fluids into Supercritical Environments," ***Comb. Sci. Tech.***, Accepted, 2005.
34. Hulka, J., and Hutt, J., "Liquid Oxygen / Hydrogen Instability Phenomena," Liquid Rocket Engine Combustion Instability, edited by V. Yang and W. Anderson, ***Progress in Astronautics and Aeronautics***, AIAA, Washington, DC, 1995, pp. 39-72.
35. Faragó, Z., and Chigier, N., "Morphological Classification of Disintegration of Round Liquid Jets in a Coaxial Air Stream," ***Atomization and Sprays***, Vol. 2, 1992, pp. 137-153.

APPENDIX

Table 1. Summary of Core Length Literature for Shear-Coaxial Jets

REF#	Author	Date	Fluid Inner Jet	Fluid Outer Jet	Fluid Ambient	Pressure (MPa)	T_i (K)	T_o (K)	T_∞ (K)
6	Forstall & Shapiro	1950	Air+ 10 %He	Air	Air	0.1*	Ambient [a]	Ambient	Ambient
7	Chigier & Beer	1964	Air	Air	Air	0.1*	Ambient	Ambient	Ambient
8	Champage& Wygnanski	1971	Air	Air	Air	0.1	Ambient	Ambient	Ambient
9	Au and Ko	1987	Air	Air	Air*	0.1*	Ambient	Ambient	Ambient
10	Eroglu et al.	1991	Water	Air	Air	0.1*	Ambient	Ambient	Ambient
11	Woodward	1993	KI (aq.)	N2, He	N2, He	0.1 - 2.17	Ambient	Ambient	Ambient
15	Villermaux et al.[g]	1994	Water	Water	Water	0.1*	Ambient	Ambient	Ambient
12	Englebert et al.	1995	Water	Air	Air	0.1	293	293 - 636	293
13	Carreau et al.	1997	LOX	He, N2, Ar	NC[c]	0.1	82[d]	245 - 272[d]	NC
16	Rehab et al.[g]	1997	Water	Water	Water	0.1*	Ambient	Ambient	Ambient
17	Rehab et al.[g]	1997	Water	Water	Water	0.1*	Ambient	Ambient	Ambient
18	Villermaux [g,h]	1998	Water	Water	Water	NR	NR	NR	NR
19	Lasheras et al.[g]	1998	Water	Air	Air	0.1	Ambient	Ambient	Ambient
20	Lasheras & Hopfinger [g,i]	2000	NR	NR	NR	NR	NR	NR	NR

21	Favre-Marinet & Schettini	2001	Air, SF6	Air,He	Air, He	0.1	Ambient	Ambient	Ambient
14	Porcheron et al.	2002	LOX, Water	He, N2, Ar, Air	Air	0.1	82, 293	245 - 293	293
This work	Davis et al.	2005	N2	N2	N2	1.4 – 4.9	108 - 133	132 - 204	197 - 249

Table 1. Summary of Core Length Literature for Shear-Coaxial Jets (continued).

REF#	Author	Density Ratio	Velocity Ratio	*M*	Re Inner	Re Outer	We
		Outer/Inner	Outer/Inner	Outer/Inner	(10^4)	(10^4)	
6	Forstall & Shapiro	1.09	0.2 - 0.75	0.04 - 0.61	NR	NR	NA
7	Chigier & Beer	1*	0.024 - 2.35	5.8e-4 - 5.52	~10 [b]	~10 [b]	NA
8	Champage & Wygnanski	1*	0 - 10	0 - 100	1.01 - 10.15	0 - 9.6	NA
9	Au and Ko	1*	1.25 - 6.67	1.5 - 44	NR	NR	NA
10	Eroglu et al.	0.001	4.5 - 131.2	0.02 - 17.2	0.15 - 0.93	2.0 - 11.6	15 - 530
11	Woodward	0.0006 - 0.018	0 - 30	0 - 1.7	7.86 - 18.9	NR	12 - 3600
15	Villermaux et al.[g]	1	1 - 6	1 - 36	>5000	>5000	NA
12	Englebert et al.	0.0008 - 0.0012	10.25 - 66.75	0.12 - 4.3	0.54 - 3.4	4.8 - 16.5	76 - 2610
13	Carreau et al.	NR	NR	3 - 21.5	5.32 - 8.11	NR	9.19×10^3 - 3.48×10^4
16	Rehab et al.[g]	1	2.2 - 5.6	4.9 - 31	1 - 10	1 - 10	NA
17	Rehab et al.[g]	1	2 - 5	4 - 25	NR[f]	NR[f]	NA
18	Villermaux [g,h]	1*	NR	NR	NR	NR	NR
19	Lasheras et al.[g]	0.001	NR	NR	NR	NR	NR
20	Lasheras & Hopfinger [g,i]	NR	NR	NR	NR	NR	NR
21	Favre-Marinet & Schettini	0.028 - 1	3.0 - 70	1 - 200	NR	3200, 11000	NA
14	Porcheron et al.	1.6×10^{-4} - 2.3×10^{-3}	NR	2 - 21.6	NR	NR	0 - 14000
This work	Davis et al.	0.04 - 0.56	1.2 - 11.1	0.19 - 11.2	1.2 - 3.2	0.8 - 19	32 - ∞

Table 1. Summary of Core Length Literature for Shear-Coaxial Jets (continued).

REF#	Author	D_1	D_2	D_3	$(D_3-D_2)/2$	Area Ratio	Post Recess	Injector
		(mm)	(mm)	(mm)	(mm)	Outer/Inner	(mm)	$Lpost/D_1$
6	Forstall & Shapiro	6.4, 25	NR	102	NR	NR	NR	NR
7	Chigier & Beer	25	64	97	16.5	8.50	0*	NR
8	Champage & Wygnanski	25	NR	NR	NR	1.28, 2.94	0*	NR
9	Au and Ko	2	2.2	4	0.9	2.79	0*	NR
10	Eroglu et al.	0.971	1.262	10.36	4.549	112.15	-0.6	57
11	Woodward	4.76	6.35	9.86	1.76	2.51	0.0	85
15	Villermaux et al.[g]	40	51	55	0.2	0.27	0*	"long"
12	Englebert et al.	2.3	2.95	14.95	6.00	40.60	0.0	22
13	Carreau et al.	5[d]	5.57[d]	16[d]	5.2[d]	9	0.0	NR
16	Rehab et al.[g]	NR	NR	NR	NR	1.82, 1.87, 5.24[e]	0*	NR
17	Rehab et al.[g]	20	21	27	3	1.82	0	NR
18	Villermaux [g,h]	NR	NR	NR	NR	NR	NR	NR
19	Lasheras et al.[g]	3.8	4.2	5.6	0.7	0.95	0	29
20	Lasheras & Hopfinger [g,i]	NR	NR	NR	NR	NR	NR	NR
21	Favre-Marinet & Schettini	20	20.4	27	3.3	0.78	0.0	6.75
14	Porcheron et al.	5, 2.1	5.57, 2.5	16, 7	2.25	9, 9.69	0*	NR
This work	Davis et al.	0.51	1.59	2.42	0.415	12.80	0.25	100

Table 1. Summary of Core Length Literature for Shear-Coaxial Jets (continued).

REF	Author	Diagnostic	Quantity	Equation
			Measured	
6	Forstall & Shapiro	Pitot tube, Sampling Tube	Potential Core	$L/D_1 = 4 + 12V_r$
7	Chigier & Beer	Pitot tube	Potential Core	
8	Champage & Wygnanski	Hot wire anemo-meter	Inner Core	
9	Au and Ko	Hot wire anemo-meter	Potential Core	
10	Eroglu et al.	Back-lit still	Liquid Intact Length	$L/D_1 = 0.66\,We^{-0.4}\,Re^{0.6}$
11	Woodward	x-ray Radio-graphy	Intact Liquid Core Length	$L/D_1 = 0.0095\left(\frac{\rho_o}{\rho_i}\right)^{\frac{-0.36}{r}} We^{-0.22/r}\,Re^{0.68}$
15	Villermaux et al. [g]	Hot film anemo-meter	Potential Core / Cone	$L/D_1 = 7/V_r$
12	Englebert et al.	Back-lit high-speed 16mm film	Breakup Length	$L/D_1 = 40\,We^{-0.27}$ $\frac{2L}{D_3 - D_2} = 10.6M_R^{-0.3} = 13.7E_R^{-0.2}$
13	Carreau et al.	Fiber optic Probe	Breakup Length, Potential Cone Length	$L/D_1 = 0.0012\left(\frac{\rho_o}{\rho_i}\right)^{-0.32} We^{-0.33}\,Re^{0.55}$
16	Rehab et al.[g]	Hot film anemo-meter	Potential Core	$L/D_1 = 6/V_r;\quad L/D_1 = 7.5/V$
17	Rehab et al.[g]	Hot-film anemo-meter, Pitot tube, LIF image	Potential Cone	$L/D_1 = 6/V_r;\ L/D_1 = 8/V$ $L/D_1 = 0.5\left(\frac{1}{(C\alpha V_r)^2} - 1\right)^{1/2} \approx \frac{1}{2C\alpha V_r}$
18	Villermaux [g,h]	[h]	Potential Cone, Liquid intact length	$L/D_1 = c/V_r;\ 6 < c < 8$

Table 1. Summary of Core Length Literature for Shear-Coaxial Jets (continued).

REF	Author	Diagnostic	Quantity	Equation
19	Lasheras et al.[g]	Photo-graph	Liquid intact length	$L/D_1 = \left(\frac{1}{4(C\alpha)^2 M} - \frac{1}{4} \right)^{1/2} \approx \frac{6}{M^{1/2}}$
20	Lasheras & Hopfinger [g,i]	[j]	[j]	$L/D_1 = \frac{1}{2cM^{2/3}} \left(\frac{\sigma}{\mu_i U_i} \right)^{1/3}$ $L/D_1 \approx \frac{6}{M^{1/2}} \left(\left\| 1 - \frac{U_i}{U_o} \right\| \right)^{-1}$ $L/D_1 \approx \frac{6}{M^{1/2}} \frac{1}{\left(1 - \frac{B\sigma}{\mu_o U_o} \right)^{0.5}}$
21	Favre-Marinet & Schettini	Aspirating Probe w/ hot-wire	Potential Core	$L/D_1 \propto M^{-0.5}$
14	Porcheron et al.	Fiber optic Probe		$L/D_1 = 2.85 \left(\frac{\rho_o}{\rho_i} \right)^{-0.32} Z^{0.34} M^{-0.13}$
This work	Davis et al.	Shadow-graph	Dark Core	$L/D_1 \approx \frac{12}{M^{1/2}}$ $L/D_1 \approx \frac{25}{M^{0.2}}$

Table 1 Notes

NR = not reported
NA = not applicable
NC = not clear from report
* assumed from the context, but not directly reported
[a] Ambient temperature assumed from the context of discussion, but generally not specifically stated in report.
[b] reported as approximately 10^5
[d] The dimensions of the injector and the temperatures were not given in the paper, but were given in the paper by Porcheron et al.[14]
[e] This number is the diameter ratio squared, which is approximately the area ratio for a very thin lip injector. The only dimensional information given was the diameter ratios (1.35, 1.37, and 2.29 mm) and the lip thickness (D2-D1) of 0.3 mm.
[f] A Re based on momentum conservation reported and defined as
Re = $\rho_o U_o D_3/\mu^*(1-(D_1/D_3))^{0.5}$ ranged from 10^4 - 10^5.
[g] These papers are from the same collaboration / research group over several years.
[h] This paper was an analysis paper that presented a different equation based on the data from the same group of researchers[15-17]
[i] This paper was a review paper encompassing the work from this same collaboration of researchers[15-19], as well as others.
[j] Unable to make measurements from images, and therefore not compared quantitatively to theory for core length.